Capacitive deionization of water involving mosaic membranes based on fibrous polymer matrices

Yurii M. Volfkovich[a,*], Nataliya A. Kononenko[b], Alexey A. Mikhalin[a], Marina M. Kardash[c], Alexey Yu. Rychagov[a], Sergei V. Tsipliaev[c], Svetlana A. Shkirskaya[b], Valentin E. Sosenkin[a]

[a]*A.N. Frumkin Institute of Physical Chemistry and Electrochemistry of RAS, Moscow, Russian Federation,*
email: yuvolf40@mail.ru (Y.M. Volfkovich)
[b]*Kuban State University, Krasnodar, Russian Federation*
[c]*Engels State Technology University, Engels, Russian Federation*

ABSTRACT

Mosaic membranes for capacitive deionization of water contained cation-exchange and anion-exchange components in matrices based on synthetic fibers. The method of the membrane preparation involved pressing of cation-exchange and anion-exchange membranes into each other - pressed membrane was obtained in this manner. Another way was the subsequent formation of the strips of cation-exchanger and anion-exchanger in the fibrous matrix (striped membrane). The specific energy consumptions were 31.9 and 111.7 Wh mol^{-1} for the assembles containing striped and pressed membranes, respectively. Thus, the striped membrane was preferable for obtaining pure drinking water.

Keywords: Mosaic ion exchange membrane; Capacitive deionization; Standard contact porosimetry; Activated carbon

1. Introduction

Among known desalination methods, baro- and electro membrane separation techniques are widely used for desalination of salt and brackish water. However, the current efficiency of electrodialysis is limited by diffusion though the solution at the membrane-liquid interface, this barrier as well as energy consumptions arise with the decrease of salt content in water being desalinated [1,2]. In this case, the energy intensity of electrodialysis can be reduced by the insertion of an ion-exchanger into the membrane system [3,4]. It should be stressed that the current efficiency strongly depends on the ion exchange filler. When water contains doubly charged ions, for instance, hardness salts, high current efficiency is achieved for flexible ion exchange resins [5,6]. Another approach that allows us to increase the current efficiency is the operation under over limiting current [7,8]. However, these conditions require considerable energy consumptions, which becomes higher with an increase in current. Moreover, damage to membranes is possible due to their local warming up [9,10].

Currently, reverse osmosis is most often applied for water desalination [11,12], it requires only high pressure and no additional expenses for electric current. Nevertheless, from an economic point of view, the method of capacitive deionization (CDI) is more attractive even than reverse osmosis, since CDI requires 3 times less energy [13,14]. The scheme of CDI processes is as follows. The aqueous solution passes through the electrochemical cell. Highly dispersive carbon electrodes are usually used. These electrodes are characterized by a high specific surface area (300–3,000 m^2 g^{-1}) [15,16]. Unlike the membrane processes, the ions are concentrated inside the electrodes. The low potential difference (slightly higher than 1.2 V) is applied, low energy consumptions are provided in this manner. The electrodes are separated

* Corresponding author.

with a porous inert spacer that is made of glass or fibrous polymer [17,18].

During the solution passage, anions are adsorbed by a positively charged electrode and cations are adsorbed by a negatively charged electrode, resulting in the desalination of the solution. Adsorption takes place since the electric double layer (EDL) is charged similarly to an electrochemical supercapacitor (ECSC) [19,20]. When the circuit is closed (the discharge of an ECSC) or reverse polarity, the ions are transferred from the solid–liquid interface back to the solution that flows out of the cell. As a result, energy regeneration and concentrating the solution occurs. The concentrating takes place since a small amount of water is supplied to the cell during the regeneration stage. After regeneration, the cell is ready to be used repeatedly for desalination. Thus, when a CDI device includes two electrochemical cells, continuous desalination can be performed (deionization occurs in the first cell, while the second cell is regenerated). The consumed energy is partially compensated by electrical energy during the regeneration stage. As a result, the CDI processes require lower energy consumption comparing with other techniques of water deionization.

One type of CDI is the method of membrane capacitive deionization (MCDI) [21–36]. Anion-exchange membranes (AEM) contacts to the positively charged electrode preventing cation transport to the anode. The cation-exchange membranes (CEM) contacts to the negatively charged electrode. Its function is to exclude the transport of anions to the cathode direction. The function of CDI is also to prevent the repulsion of co-ions from the electrodes when charging the electrode. This approach promotes the separation of oppositely charged ions in the MCDI device. The drawback of MCDI is the additional hydrodynamic resistance of the membranes, which makes its contributions to energy consumptions.

To provide the most complete desalination and reduce energy consumptions, many electrodes have been proposed for CDI: activated carbon (AC) and carbon nanomaterials [33–36] as well as the composites including them [37–40]. Spacers (porous separators) for CDI have received far less attention. However, this problem is actual, especially in the case of deepwater purification. High energy consumptions are necessary for this purpose due to the very high electrical resistance of pure water. In [41] several new spacer modifications for MCDI were developed. It should be underlined that AC electrodes possess high conductivity in pure water [42] due to surface conductivity caused by surface ion-exchange groups [43].

A membrane-electrode assembly (MEA) has been developed and investigated in [17] for CDI processes to obtain pure water. The assembly consisted of mosaic membrane (MM) and AC electrodes, which are characterized by high values of hydrophilic specific surface area and high content of oppositely charged surface groups. MM contains both cation and anion exchange groups. The energy losses for the MEA containing MM were found much less than those for the cell containing a conventional porous spacer. This is due to the high ionic conductivity of the MM at low salt concentrations. Glass fiber spacer was taken as a conventional porous spacer.

Both film and fibrous MM were applied to electrodialysis [44]. Ceramic [45,46] and polymer [47,48] membranes containing inorganic ion-exchangers [45–47], particularly amphoteric oxides of multivalent metals [45–48] were also studied.

As shown, the fibrous MM is characterized by a higher volume of macropores in comparison with the film membrane [17]. Thus, hydrodynamic permeability of the fibrous MM is higher comparing with film MM. This gives the possibility to use this membrane for CDI processes. It is known that the transport of ions through fibrous materials strongly depends on their composition and morphology [49,50]. Thus, this study aims to examine the effect of the design of fibrous MMs on characteristics of CDI under static and dynamic conditions.

2. Experimental

2.1. Synthesis of MMs

Fibrous "Polycon" MMs were prepared using the method proposed in [51,52]. Fibrous phenol-formaldehyde matrix was applied as a substrate, the ion-exchangers were inserted inside it and also coated its outer surface [52,53]. Severally CEM and AEM were manufactured. Ion exchange constituents were synthesized directly inside fibrous matrices. As a filler of the CEM, the analog of KU-1 strongly acidic resin containing –SO_3H groups was used. To obtain an AEM, the analog of EDE-10P anion exchange resin was synthesized in the matrix. This analog contains secondary, tertiary and quaternary amino groups

The membranes were thermostated at 120°C and 60 MPa [52,53]. Then the CEMs and AEMs were hot-pressed into each other. As a result, "Polycon" MM was formed, the membrane consisted of a strongly acidic cation exchanger and weakly basic anion exchanger, their mass ratio is 1:1. The thickness of the membrane was 450 microns.

Striped membrane was obtained based on the "Kynol" novolac phenol-formaldehyde fibrous matrix (KYNOL EUROPA GmbH, Germany) [54]. The same cation and anion exchange resins were applied to the matrix modification. The stripes (4 mm of thickness) were formed successively on the surface and in the bulk of the fibrous matrix. The formation was carried out directly in fibrous matrices [50,51]. First of all, cation exchange stripes were formed leaving loose strips for the subsequent formation of the anion exchange matrix. The thickness of the striped MM was 0.6 mm.

2.2. Characterization of membranes

The membranes were studied using JEOL scanning electron microscopy (SEM) (JEOL, Japan). The samples were fixed on a graphite holder using conductive tape. The samples were preliminarily coated with ultrathin graphite layer. A Crystal-45 optical microscope (Konus, USA) was also applied to investigations.

The method of standard contact porosimetry (MSCP) [55–59], which has been acknowledged by the International Union of Pure and Applied Chemistry [60], was applied to investigate the porous structure of the membranes. The MSCP gives a possibility to obtain pore size distributions in a very wide region of pore radius, namely from 1 to 10^5 nm.

The ion exchange capacity of MMs has been determined according to the method given in [17]. Electrical conductivity

was estimated from the value of membrane resistance, which was determined using impedance spectroscopy Voltalab 40 potentiostat (Radiometer Analytical, France). The frequency interval was 10^{-2}–10^6 Hz, the membrane resistance and conductivity were calculated from the wide plateau of the frequency spectra of the real part of the impedance. Mercury electrodes were used, they were in contact with the membrane [60]. Preliminarily the membrane was equilibrated with a NaCl solution, its concentration was varied from 0.01 to 0.1 M [61,62].

2.3. CDI in static cell

A static cell (without liquid flow) was applied to electrochemical measurements. The MEA was preliminarily penetrated with pure water. The cell construction and measuring method were described in [15–17]. The cell contained two identical electrodes of type Norit AC DLC Supra 30 (Cabot Corporation Foundation, Inc., Dongtanjiseong-ro 333 Hwaseong-si, Gyeonggi-do, Korea) with surface areas equal to (2.75 cm^2). Graphite current collectors were in contact with the current distributor, on which the electrodes were placed. Unlike [15,16,43,63], MMs were used instead of inert porous separator (spacer). The electrodes were made of AC (Norit DLC Supra 30 powder). The powder was mixed with a conductive filler (UM-76 carbon black, Omsktehuglerod LTD, Russia) and milled. The polymeric binder (polytetrafluoroethylene, 4 mass %) was added to the mixture. Then the mixture was pressed and dried at 120°C for 48 h. The thickness of the composite electrodes was 150 ± 10 μm, their mass was 35 mg. The cell was polarized several times at the potential diapason from –600 to 600 mV. This procedure was needed to stabilize electrochemical characteristics. Both the electrodes and MM were impregnated with twice deionized water (~1 mS cm^{-1}).

Electrochemical studies involved cyclic voltammetry using a Voltalab 40 potentiostat (Radiometer Analytical, France), galvanostatic technique, and impedance spectroscopy using the device mentioned above. The Nyquist diagrams were obtained for the frequency interval 10 kHz–10 MHz, the impedance amplitude was 50 mV.

2.4. CDI in dynamic cell

The cell construction and measuring method were described in [15–17]. Fig. 1 shows the schematics picture of the CDI electrode assembly. Disk electrodes (8 cm of diameter) made of AC cloth of CH900 type (Kuraray Company, Japan) were applied to investigations. The electrodes were inserted into a dynamic CDI cell (Samsung Electronics Co., Dongtanjiseong-ro 333 Hwaseong-si, Gyeonggi-do, Korea) [15,17]. A 0.004 M KCl solution was used for deionization. The processes were carried out at 1.2–2.0 V, the flow rate of the solution was 2.5–15 cm^3 min^{-1}.

3. Results and discussion

3.1. Morphology, porosity and ion exchange capacity of MMs

The synthesis technique affects the morphology of the membranes. Fig. 2a shows SEM images of the "Polycon"

Fig. 1. Schematics picture of the CDI electrode assembly. 1 - graphite current collectors, 2 - AC electrodes, 3 - mosaic membrane.

fibrous matrix. Uniform fibers, a thickness of which is ≈15 μm, are seen. The fibers are mainly ordered since they are bundled. The fibers in the bundles (several hundred microns) are tightly packed, pores between them are less than 10 μm. However, some fibers are outside the bundles, they are disordered. These disordered fibers are responsible for pores of several hundred microns. The bundles are intertwined: it is possible to observe both longitudinal fibers and their cross-sections in the SEM image.

Regarding the pressed MM containing ion-exchanger, transition layers between cross-sections of the bundles can be observed (Fig. 2b). These layers are the longitudinal fibers, which are coated with ion-exchange polymers. The transition layers are a result of the pressing of CEM and AEM into each other (each membrane contained 60 mass % of ion-exchanger). Large pores between the bundle and transition layers are seen. They make a sufficient contribution to the MM resistance in pure water. The outer surface of the pressed MM is coated with ion-exchange polymer (Fig. 2c). The longitudinal fibers containing ion-exchange polymer are also seen on the right side of Fig. 2d. Analysis of the SEM images shows that the pressing method provides a non-uniform structure of MM. The structure involves cation- and anion exchange regions as well as the transition layer, which is formed as a result of the compression of two membranes.

Fig. 3 shows an image of the outside surface of the pressed MM membrane obtained by an optical microscope. The fibrous structure of this membrane is visible in this photo.

The photo of the striped membrane (Fig. 4) shows alternating darker and lighter stripes (the image was obtained using an optical microscope). The darker stripes correspond to cation exchange regions, the lighter ones, which are wider then darker strips, are related to anion exchanger. The mass
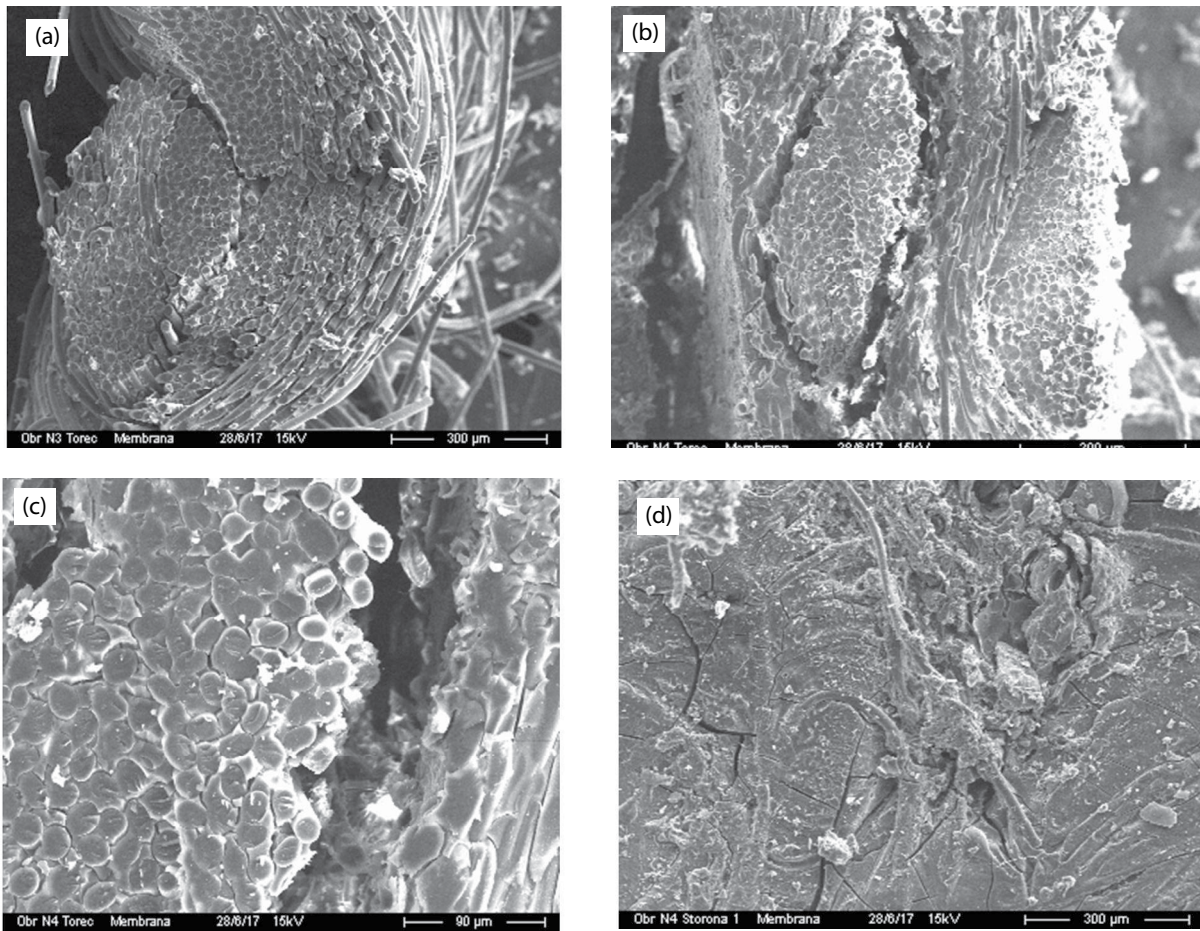
Fig. 2. SEM images of the fibrous matrix (a) and pressed MM (b–d), cross-section (a,b,d) and outer surface was studied (c).

Fig. 3. Image of outside surface of pressed MM membrane obtained by an optical microscope.

Fig. 4. Image of striped membrane obtained by an optical microscope.

ratio of cation- and anion-exchanger was 1:1, the total content of ion exchange polymer was 60%.

The values of cation (Q_c) and anion (Q_a) exchange capacity were measured for the MMs and also for AC electrodes (Table 1). The membranes and electrodes can sorb both cations and anions, it is very important for the CDI processes that provide obtaining desalinated water. Note that the higher Q_c and Q_a values have been found both for the pressed

Table 1
Cation and anion exchange capacity of AC electrodes and MMs

Sample		Q_c, mmol g^{-1}	Q_a, mmol g^{-1}
AC electrode[a]	Norit	0.56 ± 0.02	0.20 ± 0.01
	CH900	0.06 ± 0.01	0.70 ± 0.01
MM	Striped	1.00 ± 0.01	0.50 ± 0.02
	Pressed	1.50 ± 0.02	1.03 ± 0.01

[a]Data were reported earlier in [17].

and striped MMs comparing with the corresponding data for the MMs reported in [17]. The cation exchange capacity of the membranes is due to –SO$_3$ groups, anion exchangeability is caused by secondary, ternary and tertiary amino groups.

Functional groups are hydrated providing swelling of MMs in the aqueous medium. As a result, hydrophilic micro- and mesopores are formed, they are responsible for the selectivity of the membranes towards counter-ions [57,58]. When water was used as a working liquid for porosity measurements, the porous structure of ion-exchange polymers corresponds to real conditions of membrane operation. Integral and differential porosimetric curves for the fibrous MMs are shown in Fig. 5; the main data are given in Table 2. Here the micropore radii are $r < 1$ nm, the mesopore radii are 100 nm $< r < 1$ nm, the macropore radii are $r > 100$ nm.

As opposed to pressed MM, a sharp peak at log $r = 0.5$ nm is seen in differential pore size distributions for striped MM indicating regular mesopores. Regular macropores at log $r = 3.3$ (nm) have been found for the pressed MM. According

to the Kozeny equation derived for the capillary model [64], hydrodynamic permeability (K) is equal to:

$$K = \frac{Vr^2}{8} \tag{1}$$

where V is the volume of porosity (cm^3 cm^{-3}). The formula (1) is valid for straight circular capillaries of the same radius r. According to Eq. (1), hydrodynamic permeability (K) is proportional to the radius of the pores squared, therefore, the flow of the solution flows mainly through the largest pores of the membrane (i.e., macropairs), when the CDI process is carried out. As seen in Table 2, the volume of macropores of both membranes are quite large, which is suitable for CDI. These values for striped and pressed MMs are close to each other. It means that hydrodynamic flow has to be larger for a thinner membrane, that is, for the pressed MM (its thickness is 0.45 mm), whereas the thickness of the striped membrane is 0.6 mm. Since hydrodynamic permeability of the membrane determines the efficiency of CDI processes, it is desirable to manufacture thinner MMs of striped design.

3.2. Electrical conductivity of MMs affected by solution concentration

Specific electrical conductivity of pressed and striped MMs (κ_m) is plotted in Fig. 6 as a function of concentration of equilibrium solution (C). Extrapolation of the curves to the ordinate axis gives the value of conductivity in deionized water (surface conductivity, κ_s). This value depends on
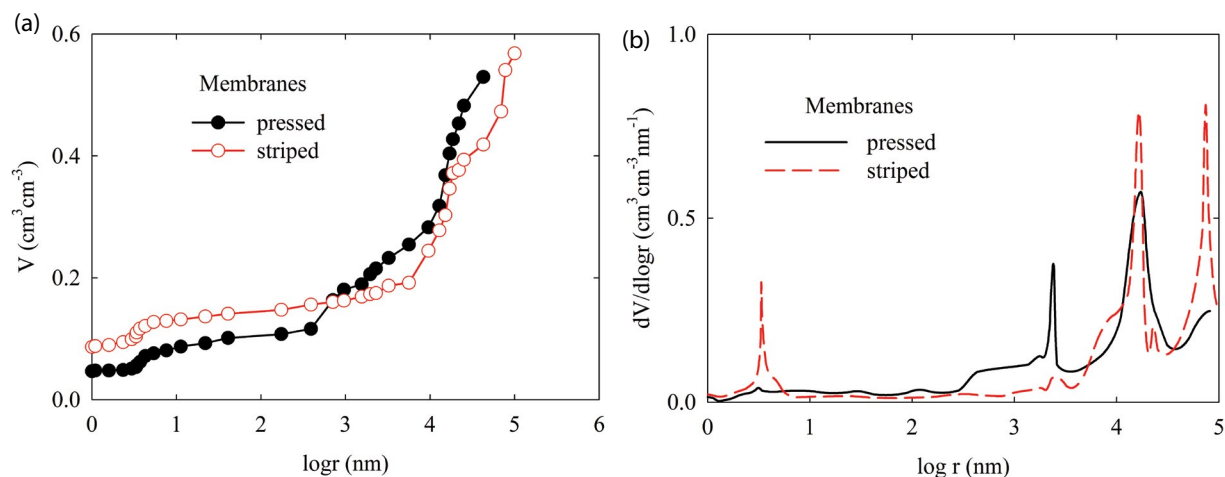
Fig. 5. Integral (a) and differential (b) pore size distributions curves for MMs swollen in water.

Table 2
Porous structure of MMs

MM	Porosity (cm^3 cm^{-3})				Specific surface area (m^2 g^{-1})
	Total	Micropores	Mesopores	Macropores	
Striped	0.57	0.09	0.06	0.42	340
Pressed	0.53	0.05	0.04	0.44	170
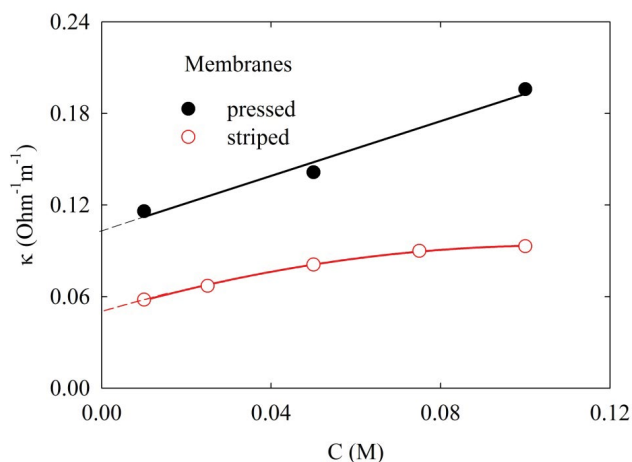
Fig. 6. Ion conductivity of MMs as a function of concentration of NaCl solution. Concentrations changed in the direction from lower concentrations to higher ones.

the content of functional groups similarly to conventional ion exchange membranes [51]. Regarding MM, the surface conductivity is determined by the total conductivity due to counter-ions of both cation- and anion-exchanger. In other words, both cations and anions are responsible for ion transport in MMs.

Considerable surface conductivity of MMs gives a possibility to use them in CDI to obtain pure water. The κ_s magnitude of the surface conductivity of a pressed membrane is substantially larger than that of a striped membrane. This is explained by higher cation- and anion exchange capacity of pressed MM comparing with the striped membrane (see Table 1).

3.3. Cyclic capacitance-voltage curves measured in pure water under static conditions

In sections 3.3 and 3.4 electrochemical studies in a static cell in which there was no flow of an aqueous solution are described. The need for these sections in this paper was caused by the two following reasons. (1) These sections are intermediate to proceeding to the next section 3.5, which describes the processes in a real dynamic electrochemical CDI cell with a solution flow. Without sections 3.3 and 3.4, it would be difficult to understand the complex electrochemical processes in a dynamic cell. (2) Since the goal of this work was to develop a CDI for producing pure water, the porous electrodes and the MM in the static cell were filled with pure water.

Fig. 7 illustrates cyclic curves, namely the dependencies of capacitance (in Farads) vs. voltage (CVF curves). The curves were plotted for different scan rates. The capacitance magnitudes were determined as $I\omega^{-1}$, where I is the current, ω is the scan rate. The curves correspond to voltammetric dependencies.

These dependencies have a shape of classical CVF curves for charging EDL of electric double-layer capacitors (DLC) with concentrated electrolytes [19,20]. As opposed to [19,20], the curves were obtained in pure water. The shape of the curves is due to the high content of ion-exchange groups in the AC electrodes and MMs. In the case of striped MM (Fig. 7a), the values of maximal specific capacitance (C) are 65 F g^{-1} (the scanning rate is 0.1 mV s^{-1}) and 45 F g^{-1} (2 mV s^{-1}).

As seen in Fig. 7b, extremes are attributed to the cyclic curves in the case of pressed membrane. The maximal specific capacitance is 60 and 30 F g^{-1}, when the scanning rate is 0.1 and 2 mV s^{-1}, respectively. A distinctive feature of these CVF curves is their deformation.

Let us compare the MEAs containing different MMs. Higher capacitance values have been obtained for the assembly with a striped membrane despite its smaller surface conductivity and larger thickness. This can be explained by the higher thickness uniformity of the structure of this MM. At the same time, the structure of the pressed MM was non-uniform. Pores between the fibers, which contained no ion-exchanger, and transition layer depressed ion transport, since the pathway of species became longer comparing with the more uniform medium.
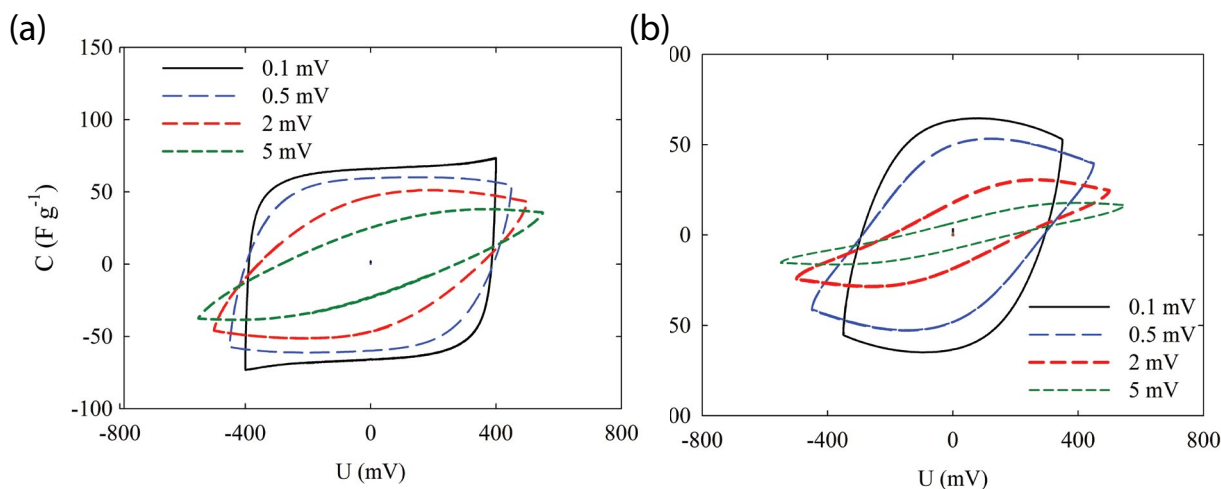
Fig. 7. Cyclic capacitance-voltage curves for striped (a) and pressed (b) membranes. The measurements were performed under static conditions.

Based on obtained here experimental data, the following operation mechanism for a static electrochemical cell containing pure water has been proposed. Counter-ions (cations) migrate through an AC electrode (anode) due to its surface conductivity [15,16,42], then their transport through a MM towards an opposite AC electrode (cathode) occurs. Simultaneously anions migrate through a cathode towards an MM, through it and in an anode. The EDL of both electrodes is charged in this manner.

3.4. Impedance measurements in static cell in pure water

Impedance investigations for static cells during long-time cycling allowed us to recognize the possible membrane degradation or the time of the stabilization of operation mode for the cell (see Fig. 8). It has been shown that the stabilization time for the total resistance of the static cell was about 30 d. Simultaneously, different types of membranes showed various behavior. Slow decrease of high-frequency resistance was characteristic of the pressed membranes. The low-frequency region was mainly determined by the electrode characteristics. During stabilization time, the cell capacitance slightly increased; this can be a result of the gradual wetting of hydrophobic pores of AC. As shown for the impedance spectrum for very low frequencies (Fig. 8b, curve 2), characteristic frequency (5 mHz) is shown. This value is attributed to the transition of the cell to the capacitive type of impedance. This frequency probably determines the time of diffusion of ions of dissociated water over the thickness of the electrodes. The main distinguishing feature of the stripe membrane is the stability of high-frequency resistance over time (Insertion of Fig. 8a). In general, it has been shown that the resistance of the pressed membrane at 10 kHz was higher in two times comparing with the stripe membrane. Comparing the impedance curves, which were

measured immediately after assembly of the cell and in a month after this, allowed us to make the following conclusion. The time to reach a steady-state in the static cell filed with pure water is too long evidently due to the very slow surface diffusion of water molecules in the hydrate shells of the counter-ions of functional groups in MMs and AC electrodes.

3.5. CDI under dynamic conditions

Comparative studies of CDI processes were also performed using a dynamic electrochemical cell to obtain deionized and concentrated water. The electrical conductivity of the aqueous solution was monitored during the stages of deionization (charging) and concentrating (discharging). The dependences of current on time (t) were also registered. Based on these data, the dependencies of concentration vs. time of deionization and concentrating were plotted for different flow rates and voltages (Fig. 9). The deionization degree ($\gamma = \dfrac{C_{ini} - C_{fin}}{C_{ini}} \times 100\%$, where the subscripts correspond to the initial and final concentrations, respectively) was also calculated for the deionization stage (Table 3).

As seen in Fig. 9 and Table 3, increasing the flow rate depresses desalination. However, the efficiency of the process increases. Increasing voltage causes the improvement of desalination (increase of the γ value).

During the regeneration stage, energy is transferred to the CDI stack partially compensating the energy for desalination. The resulting energy (W_{CDI}) is determined via [17]:

$$W_{CDI} = W_d - W_c \tag{2}$$

where W_d is the energy that is consumed for the deionization stage, W_c is the energy that transferred to the CDI stack
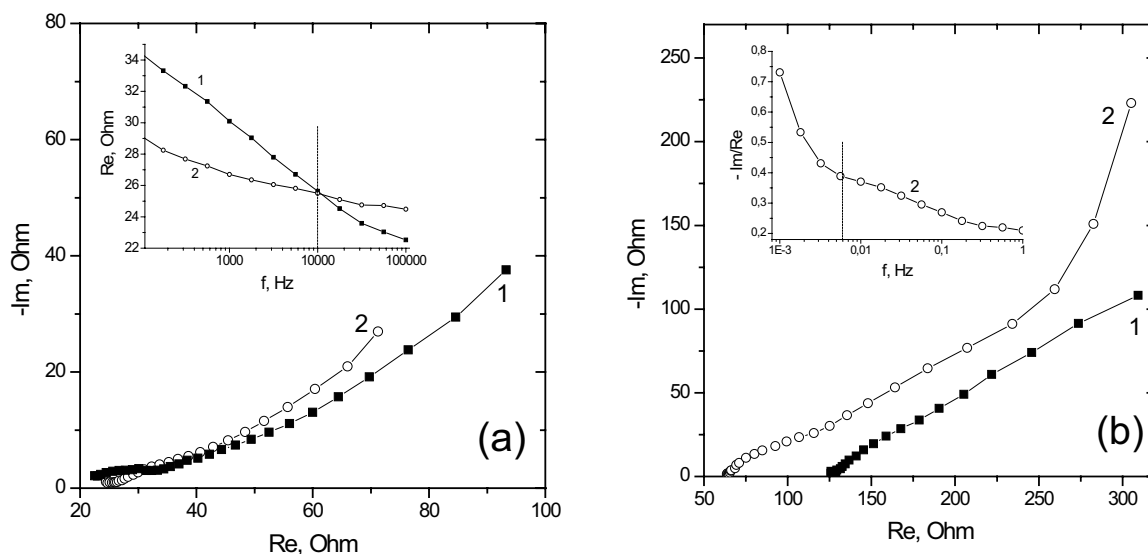
Fig. 8. Nyquist diagrams of the cell (electride/membrane/electrode) in deionized water: (a) for the stripe membrane within the frequency interval of 100 kHz to 10 mHz: 1 – the first day after the assembly, 2 – after 30 d of cathodic–anodic cycling (insertion: the dependence of real resistance on the logarithm of frequency) and (b) for pressed membrane within the frequency interval of 10 kHz to 1 mHz: 1 – first day after assembly (down to 10 mHz); 2 – after 30 d of anodic–cathodic cycling (insertion: the dependence of the ratio of capacitive and real resistances on the logarithm of frequency).
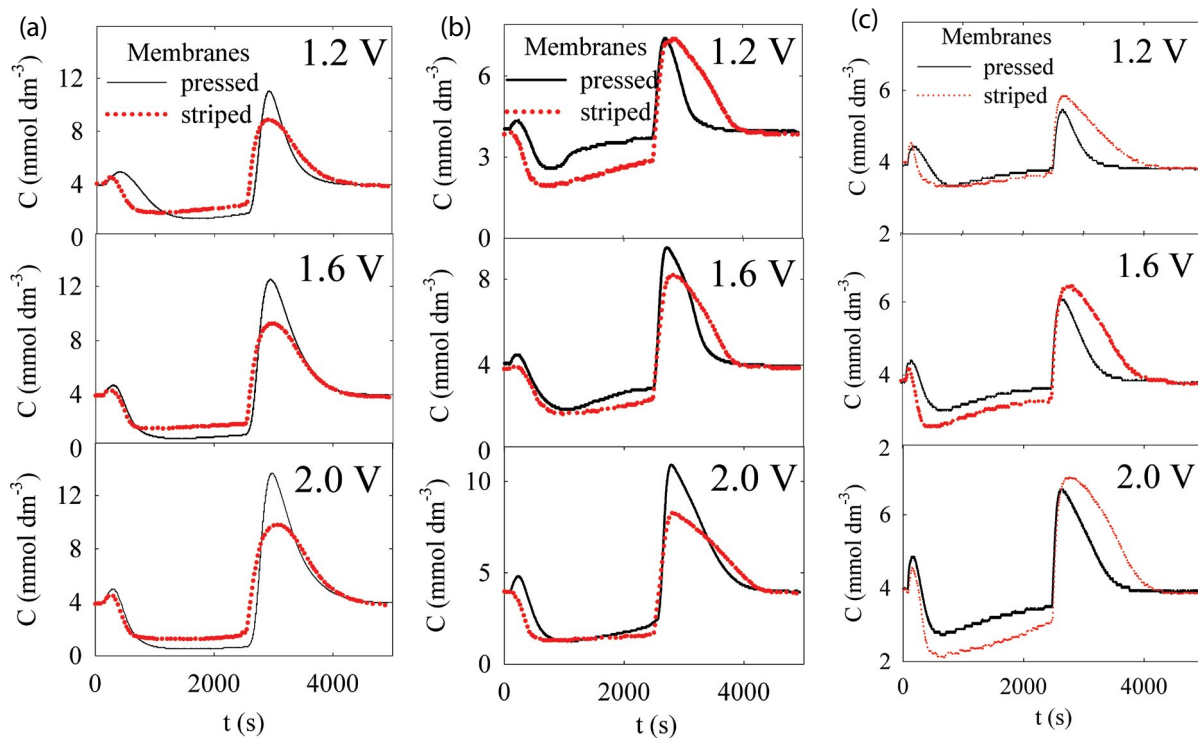
Fig. 9. Dependent of KCl concentration on time during deionization and concentrating. The flow rate of the solution was 2.5 (a), 10 (b) and 15 (c) cm^3 min^{-1}.

Table 3
Deionization degree under different voltage and flow rate

MM	υ (cm^3 m^{-1})	Desalination degree (%)				
		1.2 V	1.4 V	1.6 V	1.8 V	2 V
Pressed	2.5	62.6	77.4	81.0	85.6	86.6
Striped		54.4	59.8	62.0	65.8	67.9
Pressed	5.0	36.5	46.7	53.1	62.7	68.8
Striped		36.6	47.1	51.5	63.8	67.3
Pressed	10	36.5	46.7	53.1	62.7	68.5
Striped		49.6	53.1	55.8	57.9	67.6
Pressed	15	15.2	15.3	16.5	25.4	32.3
Striped		16.4	22.2	32.0	40.9	47.0

during regeneration. It is the W_{CDI} energy that takes into account the operation of the CDI stack since there is a gain due to energy during the regeneration stage. The energy of desalination and regeneration are calculated as:

$$W = U \int_{t_1}^{t_2} I dt \qquad (3)$$

where U is the cell voltage, t is the time.

For example Fig. 10 demonstrates current and voltage dependences on time for the deionization and regeneration stages for dynamic cell with striped MM and flow rate 10 cm^3 min^{-1}. The regeneration stage began after a short circuit in the electrical circuit. As known in the regeneration stage, energy is fed back into the electrical system [65].

Fig. 11 shows the specific energy consumption per mole of salt (W^*) absorbed on the electrodes over the desalination stage depending on voltage for different flow rates. The W^* value was calculated as:

$$W^* = \frac{W_{CDI}}{M} \qquad (4)$$

where:

$$M = \upsilon \int_{t_1}^{t_2} C dt \qquad (5)$$

where υ is the solution flow rate.

It was found that the specific energy consumption per mole of adsorbed salt was less for the pressed membrane, when the flow rate was low (2.5 cm^3 min^{-1}) (Fig. 11). Alternately, the specific energy consumption was less for the striped membrane in the case of for high flow rate (10–15 cm^3 min^{-1}) (Fig. 8). According to Fig. 9, the deionization degree was higher for the pressed MM at low flow rates; but the striped membrane showed higher g value when the solution flow was faster.

It should be noted that hydrolysis at 2 V was not observed with the evolution of gases in the tubes at the outlet of the electrochemical cell. This can be explained as follows: since the purpose of this study was to develop a method for producing pure water, in this work we used aqueous solutions with very low concentrations, therefore, with a very high electrical resistance. Thus, most of the voltage from the cell terminals was focused on the membrane.
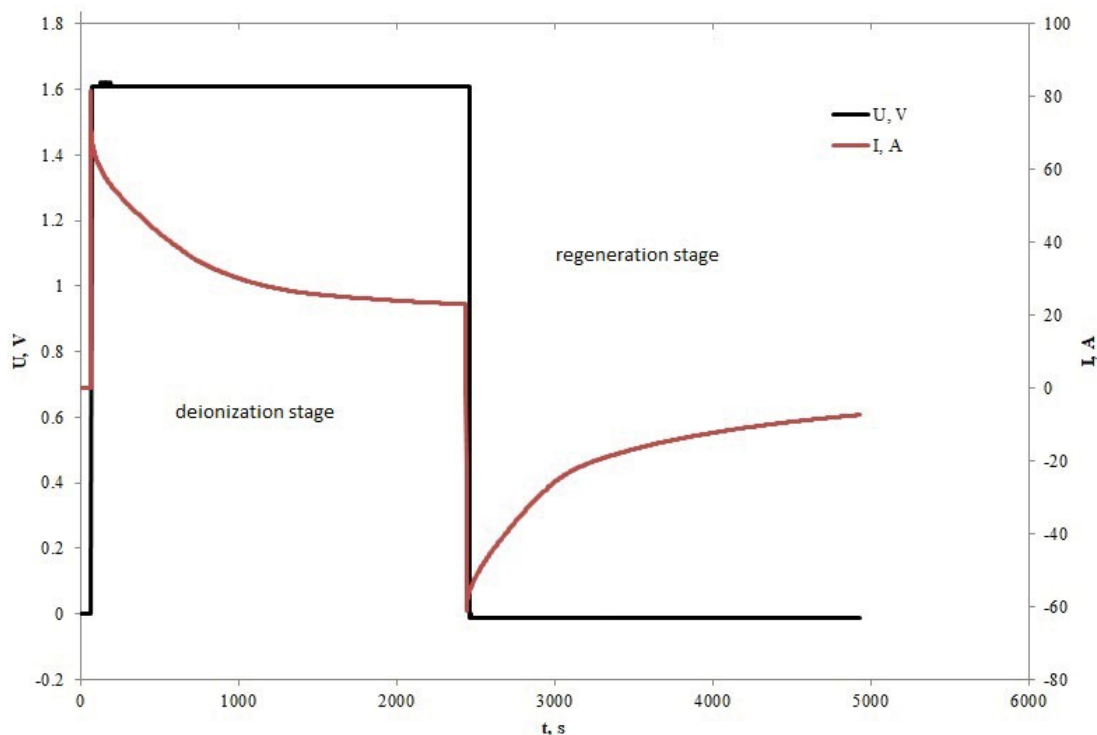
Fig. 10. Current and voltage dependences on time for the deionization and regeneration stages for dynamic cell with striped MM and flow rate 10 cm³ min⁻¹.
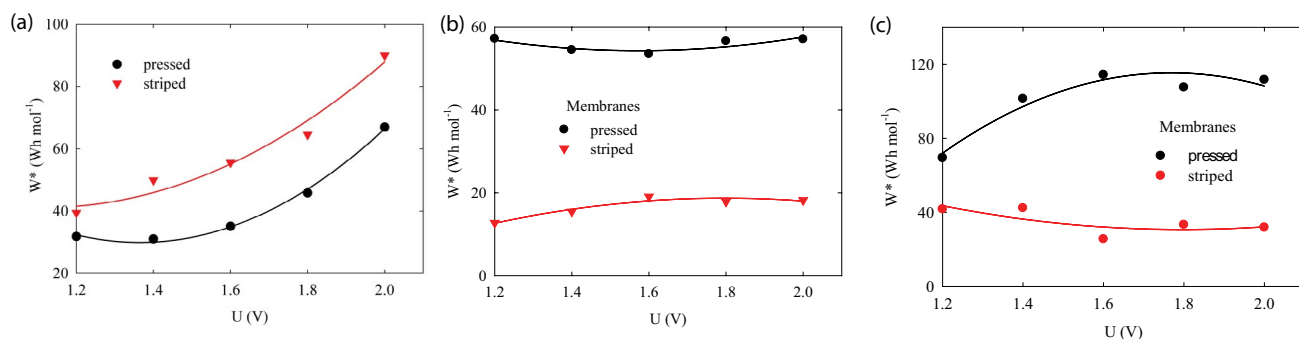
Fig. 11. The dependences of specific energy consumption on voltage. The flow rate of the solution was 2.5 (a), 10 (b) and 15 (c) cm³ min⁻¹. Voltages changed from lower to higher values.

4. Conclusions

It follows from the performed work that to obtain higher CDI characteristics for obtaining pure water, a MM should have the following properties: (1) have a uniform structure in thickness, (2) have a small thickness, and (3) provide a sufficiently high electrical conductivity at low concentrations. However, it turned out that in the laboratory MMs we made, the pressed membrane, in comparison with the striated one, had an inhomogeneous structure in thickness, smaller thickness, and greater electrical conductivity. Therefore, at low flow velocities, the main role played properties 2 and 3 and therefore pressed MM had more high characteristics. However at high flow velocities, the main role played property 1, and therefore striped MM had more

high characteristics. Since high flow rates are most favorable for obtaining of deionized water, a striped MM is more preferable than a pressed membrane. At low flow rates, the heterogeneity of the structure of the MM in thickness is not very important, since the transfer processes have time to spread over the entire thickness. However, at high flow rates, these processes do not have time to evenly spread over the entire thickness. This explains why, at low flow rates, the characteristics of CDI with pressed MM were higher than for CDI with striated MM, and at high flow rates, on the contrary, these characteristics were higher for CDI with striped MM.

The optimal conditions for desalination were as follows: the solution flow rate was 15 cm³ min⁻¹ and the voltage was 2 V. The desalination degrees were 47 and 32.3%, the specific energy consumptions were 31.9 and 111.7 Wh mol⁻¹ for

the assembles containing striped and pressed membranes, respectively. Thus, the striped membrane was preferable for obtaining pure drinking water.

Abbreviations

AEM — Anion-exchange membrane
AC — Activated carbon
CDI — Capacitive deionization
CEM — Cation-exchange membrane
ECSC — Electrochemical supercapacitor
EDL — Electric double layer
HDCE — Highly dispersive carbon electrode
MCDI — Membrane capacitive deionization
MEA — Membrane-electrode assembly
MM — Mosaic membrane
MSCP — Method of standard contact porosimetry
PMM — Pressed mosaic membrane
SC — Surface conductivity
SMM — Striped mosaic membrane

Acknowledgment

References

[1] A.M. Bernardes, M.A.S. Rodrigues, J.Z. Ferreira, Eds., Electrodialysis and Water Reuse: Novel Approaches, Springer-Verlag, Berlin, Heidelberg, 2014.

[2] H. Strathmann, Ion-Exchange Membrane processes: Their Principle and Practical Applications, Balaban Desalination Publications, Hopkinton, MA, 2016.

[3] L. Alvarado, A. Chen, Electrodeionization: principles, strategies and applications, Electrochim. Acta, 132 (2014) 583–597.

[4] J. Wood, J. Gifford, J. Arba, M. Shaw, Production of ultrapure water by continuous electrodeionization, Desalination, 250 (2010) 973–976.

[5] P.B. Spoor, L. Grabovska, L. Koene, L.J. Janssen, W.R. ter Veen, Pilot scale deionisation of a galvanic nickel solution using a hybrid ion-exchange/electrodialysis system, Chem. Eng. J., 89 (2002) 193–202.

[6] Y.S. Dzyaz'ko, L.M. Rozhdestvenskaya, A.V. Pal'chik, Recovery of nickel ions from dilute solutions by electrodialysis combined with ion exchange, Russ. J. Appl. Chem., 75 (2005) 414–421.

[7] V.V. Nikonenko, A.V. Kovalenko, M.K. Urtenov, N.D. Pismenskaya, J. Han, Ph. Sistat, G. Pourcelly, Desalination at overlimiting currents: state-of-the-art and perspectives, Desalination, 342 (2014) 85–106.

[8] V.V. Nikonenko, N.D. Pismenskaya, E.I. Belova, Ph. Sistat, P. Huguet, G. Pourcelly, Ch. Larchet, Intensive current transfer in membrane systems: modelling, mechanisms and application in electrodialysis, Adv. Colloid Interface Sci., 160 (2010) 101–123.

[9] V.I. Zabolotskiy, A.Yu. But, V.I. Vasil'eva, E.M. Akberova, S.S. Melnikov, Ion transport and electrochemical stability of strongly basic anion-exchange membranes under high current electrodialysis conditions, J. Membr. Sci., 526 (2017) 60–72.

[10] T. Sata, Ion Exchange Membranes. Preparation, Characterization, Modification and Application, RSC, Cambridge, 2004.

[11] D.M. Davenport, A. Deshmukh, J.R. Werber, M. Elimelech, High-pressure reverse osmosis for energy-efficient hypersaline brine desalination: current status, design considerations, and research needs, Environ. Sci. Technol. Lett., 5 (2018) 467–475.

[12] V.G. Good, ed., Sustainable Desalination Handbook, Plant Selection, Design and Implementation, Butterworth-Heinemann, Oxford, 2018.

[13] Y. Oren, Capacitive deionization (CDI) for desalination and water treatment—past, present and future (a review), Desalination, 228 (2008) 10–29.

[14] F.A. Al Marzooqi, A.A. Al Ghaferi, I. Saadat, N. Hilal, Application of capacitive deionisation in water desalination: a review, Desalination, 342 (2014) 3–15.

[15] Yu.M. Volfkovich, D.A. Bograchev, A.A. Mikhalin, A.Yu. Rychagov, V.E. Sosenkin, D. Park, Capacitive deionization of aqueous solutions: modeling and experiments, Desal. Wat. Treat., 69 (2017) 130–141.

[16] Yu. M. Volfkovich, D.A. Bograchev, A.A. Mikhalin, A.Yu. Rychagov, V.E. Sosenkin, V.V. Milyutin, D. Park. Electrodes based on carbon nanomaterials: structure, properties and application to capacitive deionization in static cells, Springer Proceedings in Physics, 210 (2018) 127–146.

[17] Yu.M. Volfkovich, A.Yu. Rychagov, A.A. Mikhalin, M.M. Kardash, N.A. Kononenko, D.V. Ainetdinov, S.A. Shkirskaya, V.E. Sosenkin, Capacitive deionization of water using mosaic membrane, Desalination, 426 (2018) 1–10.

[18] R. Zhao, P.M. Biesheuvel, A. van der Wal, Energy consumption and constant current operation in membrane capacitive deionization, Energy Environ. Sci., 5 (2012) 9520–9527.

[19] B.E. Conway, Electrochemical Supercapacitors: Scientific Fundamentals and Technological Applications, Springer, New York, 1999.

[20] V.S. Bagotsky, A.M. Skundin, Yu.M. Volfkovich, Electrochemical Power Sources: Batteries, Fuel Cells, Supercapacitors, John Wiley & Sons Inc., New Jersey, 2015.

[21] M.D. Andelman, Charge Barrier Flow-Through Capacitor, CA Patent 2444390, 2002.

[22] J.-B. Lee, K.-K. Park, H.-M. Eum, C.W. Lee, Desalination of a thermal power plant wastewater by membrane capacitive deionization, Desalination, 196 (2006) 125–134.

[23] P.M. Biesheuvel, A. van der Wal, Membrane capacitive deionization, J. Membr. Sci., 346 (2010) 256–262.

[24] M.A. Anderson, A.L. Cudero, J. Palma, Capacitive deionization as an electrochemical means of saving energy and delivering clean water. Comparison to present desalination practices: will it compete?, Electrochim. Acta, 55 (2010) 3845–3856.

[25] W. Tang, D. He, C. Zhang, T.D. Waite, Optimization of sulfate removal from brackish water by membrane capacitive deionization (MCDI), Water Res., 121 (2017) 302–310.

[26] A. Hassanvand, G.Q. Chen, P.A. Webley, S.E. Kentish, Improvement of MCDI operation and design through experiment and modelling: regeneration with brine and optimum residence time, Desalination, 417 (2017) 36–51.

[27] J.-S. Kim, J.-H. Choi, Fabrication and characterization of a carbon electrode coated with cation-exchange polymer for the membrane capacitive deionization applications, J. Membr. Sci., 355 (2010) 85–90.

[28] H. Li, Y. Gao, L. Pan, Y. Zhang, Y. Chen, Z. Sun, Electrosorptive desalination by carbon nanotubes and nanofibres electrodes and ion-exchange membranes, Water Res., 42 (2008) 4923–4928.

[29] J.-H. Lee, J.-H. Choi, The production of ultrapure water by membrane capacitive deionization (MCDI) technology, J. Membr. Sci., 409–410 (2012) 251–256.

[30] H. Li, L. Zou, Ion-exchange membrane capacitive deionization: a new strategy for brackish water desalination, Desalination, 275 (2011) 62–66.

[31] Y.-J. Kim, J.-H. Choi, Improvement of desalination efficiency in capacitive deionization using a carbon electrode coated with an ion-exchange polymer, Water Res., 44 (2010) 990–996.

[32] P.M. Biesheuvel, R. Zhao, S. Porada, A. van der Wal, Theory of membrane capacitive deionization including the effect of the electrode pore space, J. Colloid Interface Sci., 360 (2011) 239–248.

[33] C. Kim, P. Srimuk, J. Lee, S. Fleischmann, M. Aslan, V. Presser, Influence of pore structure and cell voltage of activated carbon cloth as a versatile electrode material for capacitive deionization, Carbon, 122 (2017) 329–335.

[34] J. Cao, Y. Wang, C. Chen, F. Yu, J. Ma, A Comparison of graphene hydrogels modified with single-walled/multi-walled carbon

nanotubes as electrode materials for capacitive deionization, J. Colloid Interface Sci., 518 (2018) 69–75.

[35] Y.M. Volfkovich, D.A. Bograchev, A.M. Mikhalin, A.Yu. Rychagov, V.E. Sosenkin, V.V. Milyutin, D. Park, Electrodes Based on Carbon Nanomaterials: Structure, Properties and Application to Capacitive Deionization in Static Cells, Chapter 9, O. Fesenko, L. Fesenko, Eds., Nano-Optics, Nanophotonics, Nanomaterials, and Their Applications, Springer, 2018, pp. 127–139.

[36] J. Feng, Z. Yang, S. Hou, M. Li, R. Lv, F. Kang, Z-H. Huang, GO/auricularia - derived hierarchical porous carbon used for capacitive deionization with high performance, Colloids Surf., A, 547 (2018) 134–140.

[37] M.S. Gaikwad, C. Balomajumder, Polymer coated capacitive deionization electrode for desalination: a mini review, Electrochem. Energy Technol., 2 (2016) 1–5.

[38] Y. Liu, C. Nie, X. Liu, X. Xu, Z. Sun, L. Pan, Review on carbon-based composite materials for capacitive deionization, RSC Adv., 5 (2015) 15205–15225.

[39] D. Zhang, X. Wen, L. Shi, T. Yan, J. Zhang, Enhanced capacitive deionization of graphene/mesoporous carbon composites, Nanoscale, 4 (2012) 5440–5446.

[40] M.T.Z. Myint, J. Dutta, Fabrication of zinc oxide nanorods modified activated carbon cloth electrode for desalination of brackish water using capacitive deionization approach, Desalination, 305 (2012) 24–30.

[41] Y. Bian, P. Liang, X. Yang, Y. Jiang, C. Zhang, X. Huang, Using activated carbon fiber separators to enhance the desalination rate of membrane capacitive deionization, Desalination, 381 (2016) 95–99.

[42] Yu.M. Volfkovich, A.A. Mikhalin, A.Y. Rychagov, Surface conductivity measurements for porous carbon electrodes, Russ. J. Electrochem., 49 (2013) 594–599.

[43] Yu.M. Volfkovich, D.A. Bograchev, A.Yu. Rychagov, V.E. Sosenkin, M.Yu. Chaika, Supercapacitors with carbon electrodes. Energy efficiency: modeling and experimental verification, J. Solid State Electrochem., 19 (2015) 1–9.

[44] N.P. Berezina, N.A. Kononenko, Yu.M. Volfkovich, Yu. G. Freidlin, L.G. Chernoskutova, Physico-chemical properties of aniono-cationo exchange membranes of mosaic structure, J. Soviet Electrochem., 29 (1989) 912–915.

[45] J. Mora-Gomez, M. Garcia-Gabaldon, M.C. Marti-Catalayud, S. Mestre, V. Perez-Herranz, Anion transport through ceramic electrodialysis membranes made with hydrated cerium dioxide, J. Am. Ceram. Soc., 100 (2017) 4180–4189.

[46] Y.S. Dzyazko, A.S. Rudenko, Y.M. Yukhin, A.V. Palchik, V.N. Belyakov, Modification of ceramic membranes with inorganic sorbents. Application to electrodialytic recovery of Cr(VI) anions from multicomponent solution, Desalination, 342 (2014) 52–60.

[47] R. Pang, X. Li, J. Li, Z. Lu, X. Sun, L. Wang, Preparation and characterization of ZrO$_2$/PES hybrid ultrafiltration membrane with uniform ZrO$_2$ nanoparticles, Desalination, 332 (2014) 60–66.

[48] Y.S. Dzyazko, L.M. Rozhdestvenskaya, Y.G. Zmievskii, A.I. Vilenskii, V.G. Myronchuk, L.V. Kornienko, S.L. Vasilyuk, N.N. Tsyba, Organic-inorganic materials containing nanoparticles of zirconium hydrophosphate for baromembrane separation, Nanoscale Res. Lett., 10 (2015) 1–11.

[49] R.J. Phillips, W.M. Deen, J.F. Brady, Hindered transport of spherical macromolecules in fibrous membranes and gels, AIChE J., 35 (1989) 1761–1769.

[50] A.I. Gopalan, K.-P. Lee, K.M. Manesha, P. Santhosh, Poly (vinylidene fluoride)–polydiphenylamine composite electrospun membrane as high-performance polymer electrolyte for lithium batteries, J. Membr. Sci., 318 (2008) 422–428.

[51] M.M. Kardash, Yu.M. Vol'fkovich, I.A. Tyurin, N.A. Kononenko, D.V. Oleinik, M.A. Chernyaeva, Effect of process parameters of manufacturing of composite fibrous membranes on their structure and ion selectivity, Petrol. Chem., 53 (2013) 482–488.

[52] M.M. Kardash, D.V. Terin, Search for a technological invariant and evolution of the structure – property relation for Polikon materials, Petrol. Chem., 56 (2016) 413–422.

[53] M.M. Kardash, N.B. Fedorchenko, O.V. Epancheva, Structural features of composite chemisorption fibre materials from polycondensation filling, Fibre Chem., 34 (2002) 466–469.

[54] http://www.kynol.de/pdf/

[55] Yu.M. Volfkovich, V.S. Bagotzky, The method of standard porosimetry 2. Investigation of the formation of porous structures, J. Power Sources, 48 (1994) 339–348.

[56] Yu.M. Volfkovich, A.V. Sakars, A.A. Volinsky, Application of the standard porosimetry method for nanomaterials, Int. J. Nanotechnol., 2 (2005) 292–302.

[57] Yu.S. Dzyazko, L.N. Ponomaryova, Yu.M. Volfkovich, V.E. Sosenkin, V.N. Belyakov, Polymer ion-exchangers modified with zirconium hydrophosphate for removal of Cd^{2+} ions from diluted solutions, Sep. Sci. Technol., 48 (2013) 2140–2149.

[58] Yu.M. Volfkovich, A.N. Filippov, V.S. Bagotsky, Structural Properties of Porous Materials and Powders Used in Different Fields of Science and Technology, Springer, 2014.

[59] N.A. Kononenko, M.A. Fomenko, Yu.M. Volfkovich, Structure of perfluorinated membranes investigated by method of standard contact porosimetry, Adv. Colloid Interface Sci., 222 (2015) 425–435.

[60] J. Rouquerol, G. Baron, R. Denoyel, H. Giesche, J. Groen, P. Klobes, P. Levitz, A.V. Neimark, S. Rigby, R. Skudas, K. Sing, M. Thommes, K. Unger, Liquid intrusion and alternative methods for the characterization of macroporous materials (IUPAC Technical Report), Pure Appl. Chem., 84 (2011) 107–136.

[61] A.B. Yaroslavtsev, Ed., Membranes and Membrane Technologies, Nauchnii Mir, Moscow, 2013 [in Russian].

[62] N.P. Gnusin, N.P. Berezina, O.A. Dyomina, N.A. Kononenko, Physicochemical principles of testing ion-exchange membranes, Russ. J. Electrochem., 32 (1996) 154–163.

[63] Yu.M. Volfkovich, D.A. Bograchev, A.A. Mikhailin, V.S. Bagotzky, Supercapacitor carbon electrodes with high capacitance, J. Solid State Electrochem., 18 (2014) 1351–1363.

[64] J. Kozeny, Uber die kapillare Leitung des Wassers im Boden, Aufstieg Versickerung und Anwendung auf die Bewasserung. Sitzungsber Akad. Wiss., Wien, 136 (1927) 271–306.

[65] J. Kang, T. Kim, H. Shin, J. Lee, J.-I. Ha, J. Yoon, Direct energy recovery system for membrane capacitive deionization, Desalination, 398 (2016) 144–150.